

Expected Improvement via Gradient Norms

Joshua Hang Sai Ip¹ Georgios Makrygiorgos¹ Ali Mesbah¹

Abstract

Bayesian Optimization (BO) is a principled approach for optimizing expensive black-box functions, with Expected Improvement (EI) being one of the most widely used acquisition functions. Despite its empirical success, EI is known to be overly exploitative and can converge to suboptimal stationary points. We propose Expected Improvement via Gradient Norms (EI-GN), a novel acquisition function that applies the improvement principle to a gradient-aware auxiliary objective, thereby promoting sampling in regions that are both high-performing and approaching first-order stationarity. EI-GN relies on gradient observations used to learn gradient-enhanced surrogate models that enable principled gradient inference from function evaluations. We derive a tractable closed-form expression for EI-GN that allows efficient optimization and show that the proposed acquisition is consistent with the improvement-based acquisition framework. Empirical evaluations on standard BO benchmarks demonstrate that EI-GN yields consistent improvements against standard baselines. We further demonstrate applicability of EI-GN to control policy learning problems.

1. Introduction

Bayesian Optimization (BO) has emerged as a popular black-box optimization method for a variety of applications such as materials discovery (Lookman et al., 2019), robotics (Calandra et al., 2016), and machine learning hyperparameter optimization (Wu et al., 2019). It relies on probabilistic surrogates, which facilitate the balance between exploration and exploitation for suggesting new queries through acquisition functions (AFs).

BO is traditionally performed derivative-free, or without the gradient information of the objective (Shahriari et al., 2015;

¹Department of Chemical and Biomolecular Engineering, University of California, Berkeley, CA, USA. Correspondence to: Joshua Hang Sai Ip <ipjoshua@berkeley.edu>.

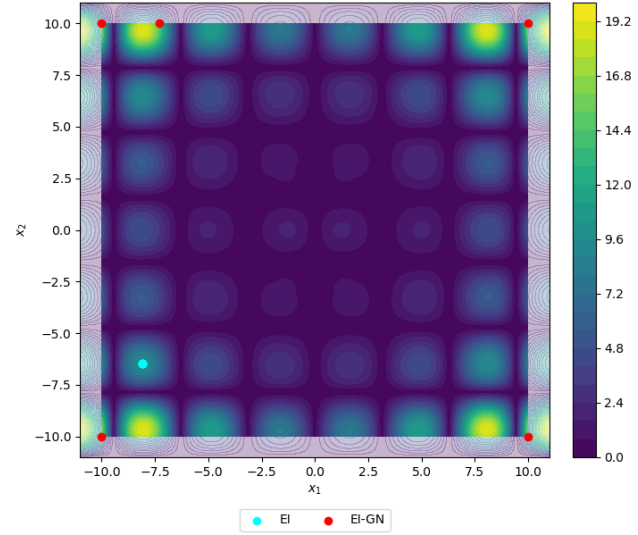


Figure 1. Five largest solutions found by EI (cyan) and the proposed acquisition function EI-GN (red) for the Holder Table function in $\mathbf{x} \in [-10, 10]^2$. EI gets trapped in one of the many local maxima and repeatedly suggests the same query, whereas EI-GN undergoes informed exploration to identify various solutions with higher objective values.

Frazier, 2018). This assumption has been revisited, notably in Wu et al. (2017), given that gradient observations are obtainable in many real-world applications at negligible additional cost (e.g., via adjoint methods in PDE-constrained optimization). However, the majority of literature on gradient-enhanced BO has focused on embedding gradients in the probabilistic surrogate model of the objective to enhance its accuracy, which can become prohibitively costly due to mapping correlations between all dimensions. There has been limited work in exploiting gradient information in the AF. In fact, posterior gradients can be leveraged directly in AF optimization just like their zeroth-order counterparts to suggest new points of query.

Expected Improvement (EI) (Jones et al., 1998) is arguably the most popular variant of AFs, though it is known to be myopic and gets stuck in local optima. EI is also known to create many regions with near-zero acquisition mass due to how the improvement criterion is constructed (Ament et al., 2023), thereby creating difficulties in finding the queries that maximize EI. The premise of this work is that gradients

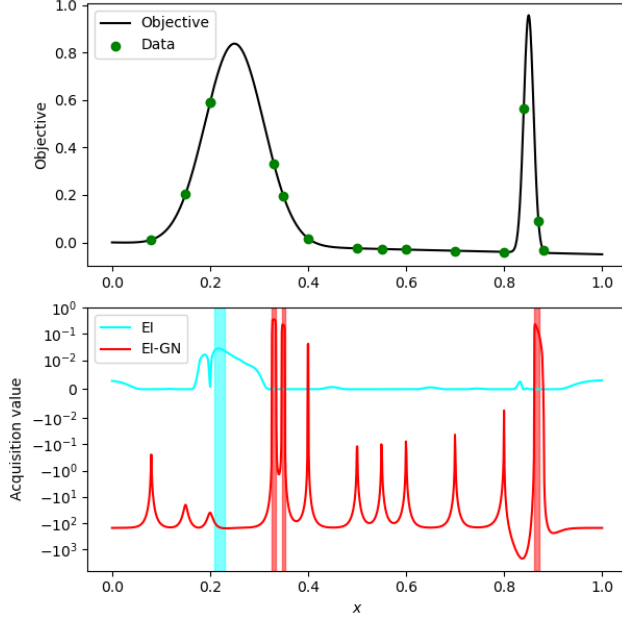


Figure 2. Comparison of acquisition behavior for a univariate mixture of Gaussians with a wide local basin and a narrow basin containing the global maximum in $x \in [0, 1]$. **Top:** Objective landscape and sampled data for GP learning. **Bottom:** Acquisition values for EI (cyan) and EI-GN (red) with regions corresponding to large values shaded.

of the objective can lead to structured exploration by providing a denser AF landscape, alleviating EI’s weakness of exploiting local optima.

Figure 1 shows the performance of EI in comparison with our proposed method, Expected Improvement via Gradient Norms (EI-GN), on maximization of the Holder Table function (Jamil & Yang, 2013), where the five largest solutions are displayed. As shown, EI repeatedly queries the same location after finding a sufficiently large local maxima, whereas EI-GN undergoes more exploration to derive distinct queries with greater objective values.

EI’s overexploitation behavior can be explained by observing the AF for a univariate mixture of Gaussians $f(\mathbf{x}) = 0.85 \exp(-0.5((\mathbf{x} - 0.25)/0.06)^2) + \exp(-0.5((\mathbf{x} - 0.85)/0.01)^2) - 0.05\mathbf{x}$, as seen in Figure 2. The top plot shows a wide basin with a local maxima and a narrow basin containing the global maxima. Gaussian Processes (GPs) are trained on the same samples and used for acquisition evaluation in EI (cyan) and EI-GN (red) in the bottom plot, where shaded regions indicate the largest acquisition values. Here, EI is approximately zero for most of the domain and its maximum lies in the local basin; this indicates EI concentrates the acquisition signal around the local maxima and not incentivized to explore. EI-GN instead produces multiple acquisition peaks, two of which corresponding to the local basin. The last one corresponds to the global basin

and facilitates less exploitative global search.

The contributions of this paper are as follows:

- We propose a novel AF, denoted by EI_g , that augments EI with a stationarity penalty derived from gradient information, encouraging structured exploration for when standard EI becomes near-zero. As seen in Figure 1, this prevents myopic behavior due to overexploitation in EI.
- We derive a lower bound for EI_g and analyze its behavior compared to EI. This analysis motivates EI-GN, a tractable AF that instantiates the same principles and admits a closed-form expression under Gaussian posteriors for practical optimization.

2. Background

2.1. Problem Formulation

We seek to maximize an expensive black-box objective $f(\mathbf{x})$

$$\mathbf{x}^* \leftarrow \arg \max_{\mathbf{x} \in \mathcal{X}} f(\mathbf{x}), \quad (1)$$

where $\mathbf{x} \in \mathbb{R}^d$. We observe potentially noisy values of the objective f and its gradients ∇f as y and ∇y , respectively. We assume that gradient observations can be obtained at negligible additional cost compared to evaluating f .

2.2. Gaussian Processes

GPs are typically the surrogate model of choice in BO due to their smoothness and non-parameteric nature, allowing flexibility in modeling objectives under minimal assumptions (Williams & Rasmussen, 2006). Let $\mathbf{X} = [\mathbf{x}_1, \dots, \mathbf{x}_N]^\top$, $\mathbf{y} = [y_1, \dots, y_N]^\top$, and $\nabla \mathbf{y} = [\nabla y_1, \dots, \nabla y_N]^\top$, where N denotes the number of samples. The posterior mean and variance for the objective can be described as

$$\mu(\mathbf{x}) = m(\mathbf{x}) + k(\mathbf{x}, \mathbf{X})K^{-1}(y - m(\mathbf{X})), \quad (2)$$

$$\sigma(\mathbf{x})^2 = k(\mathbf{x}, \mathbf{x}) - k(\mathbf{x}, \mathbf{X})K^{-1}k(\mathbf{X}, \mathbf{x}), \quad (3)$$

where $m(\cdot)$ and $k(\cdot, \cdot)$ denote the mean and kernel function, and $K = k(\mathbf{X}, \mathbf{X}) + \sigma_n^2 I$.

2.3. Expected Improvement

There is a vast body of literature on different AFs that balance exploration and exploitation, ranging from decision-theoretic approaches such as Knowledge Gradient (Wu & Frazier, 2016) to information-centric approaches such as Entropy Search (Hernández-Lobato et al., 2016). We direct our attention to EI (Jones et al., 1998), which is defined as $\text{EI}(\mathbf{x}) = \mathbb{E}[\max(f(\mathbf{x}) - f(\mathbf{x}^+), 0)]$. Since EI only considers domains that lead to improvement over $f(\mathbf{x}^+)$, the AF

value can reduce to zero for large subsets of the search space, leading to over-exploitation (Qin et al., 2017; De Ath et al., 2021). Hoffman et al. (2011) proposed portfolio allocation with different probabilities of selecting various AFs, Qin et al. (2017) suggested a stochastic non-greedy selection for EI, and Benjamins et al. (2023) used adaptive weights in EI to balance exploration and exploitation. In contrast, our proposed method directly reshapes the AF landscape by incorporating gradient information.

3. Related Work

3.1. Gradient-enhanced Gaussian Processes

There has been work extending GPs to gradient observations (Solak et al., 2002), showing gradients are beneficial in BO (Shekhar & Javidi, 2021). Wu et al. (2017) suggested a joint GP model, where every f and ∇f is correlated, though this led to prohibitively expensive complexity $\mathcal{O}((d+1)^3 N^3)$. This motivated approximations that leverage variational inference and inducing points (Padidar et al., 2021), as well as gradient-enhanced BNNs (Makrygiorgos et al., 2025). In this work, gradients are used for acquisition shaping rather than improving the surrogate of f .

3.2. Gradient-enhanced Acquisition Functions

There has been work on gradient-enhanced AFs. Makrygiorgos et al. (2023a) formulated a multi-objective AF consisting of zeroth-order and first-order terms, where multi-objective optimization leads to a Pareto frontier in the acquisition ensemble. In contrast, we define a single scalar EI-style acquisition on an auxiliary objective that integrates stationarity as a soft penalty, rather than considering trade-offs between zeroth- and first-order AFs. This maintains the global improvement structure of EI, while providing valuable acquisition shaping for when standard EI becomes near-zero in the search space.

Another line of work considers first-order optimality more explicitly. Penubothula et al. (2021) directly searched for points that correspond to objective gradients approximately equal to zero, then utilized the “significance” criterion to evaluate candidate points. Makrygiorgos et al. (2023b) enforced constraints akin to first-order optimality conditions directly in the AF for restricting search space. Our work differs from these approaches, as we do not impose constraints nor attempt to locate stationary points; we use gradient information inside the EI framework to guide AF optimization. This preserves EI’s improvement-centric behavior, while providing additional acquisition signal for when standard EI over-exploits.

Algorithm 1 Expected Improvement via Gradient-Norms

```

1: Input: Number of iterations  $T$ , search space  $\mathcal{X}$ , black-
   box objective  $(f, \nabla f)^\top$ , EI-GN penalty weight  $\alpha$ 
2: Output: Optimal decision variables  $\mathbf{x}^*$ 
3: Initialize dataset  $\mathcal{D}_0 \leftarrow (\mathbf{X}_0, \mathbf{y}_0, \nabla \mathbf{y}_0)$ 
4: for  $t = 1$  to  $T$  do
5:   Fit GP surrogate model on  $(\mathbf{X}_t, \mathbf{y}_t)$ 
6:   Fit gradient GP models on  $(\mathbf{X}_t, \nabla \mathbf{y}_t)$ 
7:   Compute  $\text{EI}_f(\mathbf{x}) = \mathbb{E}[\max(f(\mathbf{x}) - f(\mathbf{x}^+), 0)]$ 
8:   Compute  $\bar{\text{EI}}_s(\mathbf{x})$  from (11)
9:    $\mathbf{x}_{t+1} \leftarrow \arg \max_{\mathbf{x} \in \mathcal{X}} \text{EI-GN}(\mathbf{x})$  from (12)
10:  Evaluate  $(y_{t+1}, \nabla y_{t+1})^\top$ 
11:   $\mathcal{D}_{t+1} \leftarrow \mathcal{D}_t \cup \{(\mathbf{x}_{t+1}, y_{t+1}, \nabla y_{t+1})\}$ 
12: end for
13: return  $\mathbf{x}^* \leftarrow \arg \max_{(\mathbf{X}, \mathbf{y}) \in \mathcal{D}_T} \mathbf{y}$ 

```

3.3. Local Bayesian Optimization via Gradient Descent

BO is used to facilitate gradient descent by designing AFs that query points that reduce uncertainty in gradient inference (Müller et al., 2021). This notion has been extended to optimize for gradient descent direction (Nguyen et al., 2022), and gradient descent in multiple objectives (Ip et al., 2024; 2025). These works infer gradients from zeroth-order function observations for performing local optimization via gradient descent. Our method instead uses gradients to directly reshape the AF for gradient-enhanced global optimization.

4. Method

4.1. Model

Our goal is to analyze the role of gradients in providing an auxiliary signal in the acquisition landscape. To avoid confounding acquisition effects with surrogate modeling, we learn a GP for f and d independent GPs based on the objective’s partial derivatives. Hence, this allows us to avoid cross-variances between f and ∇f , as well as correlations between individual dimensions in ∇f . Consequently, the surrogate for f is identical to the one used in vanilla BO, ensuring any potential gains in optimization are solely due to acquisition behavior. The choice of uncorrelated models for f and ∇f reduces complexity to $\mathcal{O}((d+1)N^3)$. If models are trained in parallel, this further reduces complexity to $\mathcal{O}(N^3)$, independent of d . We model each partial gradient using similar equations to (2) and (3), except each dimension has its mean and kernel functions. We shall denote the posterior gradient mean and covariance as μ^∇ and Σ^∇ , respectively.

4.2. Expected Improvement on Auxiliary Objective

Inspired by Sobolev norms, we define an auxiliary function $g(\mathbf{x})$ that augments $f(\mathbf{x})$ with an additional gradient term $\|\nabla f(\mathbf{x})\|_2^2$

$$g(\mathbf{x}) = f(\mathbf{x}) - \alpha \|\nabla f(\mathbf{x})\|_2^2, \quad (4)$$

where $\alpha \geq 0$ is a hyperparameter that determines the weight of the gradient norm term in $g(\mathbf{x})$. To build intuition for how maximizing g can preserve optima of f , consider the idealized smooth setting where f attains a global maximizer $\mathbf{x}^* \in \text{int}(\mathcal{X})$ such that $\nabla f(\mathbf{x}^*) = \mathbf{0}$. This results in $g(\mathbf{x}^*) = f(\mathbf{x}^*)$, where \mathbf{x}^* is also a global maximizer of g . We note that the interior maximizer condition may not hold in practice.

The motivation for (4) is derived from the first-order necessary conditions for optimality (Boyd & Vandenberghe, 2004), where interior optima must respect stationarity conditions. Therefore, the gradient term can be considered as a soft penalty for deviations from stationarity, rather than explicit enforcement of Karush-Kuhn-Tucker (KKT) conditions. Unlike hard constraints, the soft penalty implicitly biases search away from regions that are highly non-stationary, facilitating continued exploration even when local basins that satisfy first-order optimality conditions are sparse. We define EI for $g(\mathbf{x})$ and denote it as EI_g , i.e.,

$$\text{EI}_g(\mathbf{x}) = \mathbb{E} [\max(g(\mathbf{x}) - g(\mathbf{x}^+), 0)], \quad (5)$$

where \mathbf{x}^+ denotes the decision variables corresponding to the incumbent in g .

4.3. Lower Bound of EI_g

Computing (12) does not admit a closed-form expression due to the coupling of function values and gradient norms in $g(\mathbf{x})$. Therefore, we separate the zeroth-order and first-order terms and apply the Positive Part Inequality (Lemma A.1) to derive a lower bound

$$\text{EI}_g(\mathbf{x}) \geq \text{EI}_f(\mathbf{x}) - \alpha \text{EI}_s(\mathbf{x}), \quad (6)$$

where EI_f denotes EI defined on the objective f ; akin to standard EI. EI_s is defined as

$$\text{EI}_s(\mathbf{x}) = \mathbb{E}[\max(\|\nabla f(\mathbf{x})\|_2^2 - \|\nabla f(\mathbf{x}^+)\|_2^2, 0)], \quad (7)$$

which is an EI-style improvement term in stationarity. The lower bound in (6) enables us to isolate the zeroth-order term from the first-order term. In fact, this lower bound is consistent with the original formulation of $g(\mathbf{x})$ in (4), where (6) reduces to EI when $\alpha = 0$. The derivation of (6) can be found in Appendix B.1.

4.4. Acquisition Signal in Low-Improvement Regions

We now explain why EI_g provides acquisition signal in low-improvement regions, and why this persists when optimizing its lower bound (6). Improvement in g decomposes as

$$\begin{aligned} g(\mathbf{x}) - g(\mathbf{x}^+) &= \underbrace{(f(\mathbf{x}) - f(\mathbf{x}^+))}_{\text{objective change}} \\ &\quad - \alpha \underbrace{(\|\nabla f(\mathbf{x})\|_2^2 - \|\nabla f(\mathbf{x}^+)\|_2^2)}_{\text{stationarity change}}. \end{aligned} \quad (8)$$

This reveals two pathways to improvement: (i) $f(\mathbf{x})$ exceeds $f(\mathbf{x}^+)$, the standard EI mechanism, or (ii) $\|\nabla f(\mathbf{x})\|_2^2 < \|\nabla f(\mathbf{x}^+)\|_2^2$, i.e., the gradient norm is smaller than the incumbent's, contributing positively even if $f(\mathbf{x}) < f(\mathbf{x}^+)$. Crucially, pathway (ii) can yield $g(\mathbf{x}) > g(\mathbf{x}^+)$ even when $f(\mathbf{x}) < f(\mathbf{x}^+)$; acquisitions based only on zeroth-order improvement (such as EI on f) only have access to pathway (i). To quantify when stationarity improvement guarantees progress in g , we define an event, capturing the trade-off between objective loss and gradient reduction

$$\begin{aligned} \mathcal{E}_{\delta,c}(\mathbf{x}) &= \{\|\nabla f(\mathbf{x})\|_2^2 \leq \|\nabla f(\mathbf{x}^+)\|_2^2 - \delta\} \\ &\cap \{f(\mathbf{x}) \geq f(\mathbf{x}^+) - \alpha c \delta\}, \end{aligned} \quad (9)$$

where $\delta > 0$ is a stationarity margin in units of squared gradient norm: it sets the threshold for the required stationarity decrease below $\|\nabla f(\mathbf{x}^+)\|_2^2$ in (9) and $c \in (0, 1)$ is the tolerated fraction of stationarity improvement in exchange with objective decrease. On this event, stationarity improves by at least δ , while objective drops by at most $\alpha c \delta$, so the stationarity contribution $\alpha \delta$ outweighs the objective loss. Hence, $\mathcal{E}_{\delta,c}(\mathbf{x})$ applied to (8) yields $g(\mathbf{x}) - g(\mathbf{x}^+) \geq -\alpha c \delta + \alpha \delta = \alpha(1 - c)\delta$. Consequently, $\text{EI}_g(\mathbf{x}) \geq \alpha(1 - c)\delta \mathbb{P}(\mathcal{E}_{\delta,c}(\mathbf{x}))$, so EI_g can remain informative even when $\mathbb{P}(f(\mathbf{x}) > f(\mathbf{x}^+)) \approx 0$.

The lower bound (6) retains the standard EI mechanism via EI_f , but is conservative with respect to stationarity. This is due to EI_s only penalizing upward excursions of $\|\nabla f(\mathbf{x})\|_2^2$ relative to the incumbent and not directly rewarding gradient norm decreases. In low-improvement regions where $\text{EI}_f(\mathbf{x}) \approx 0$, maximizing the EI_g lower bound (6) is approximately equivalent to minimizing $\text{EI}_s(\mathbf{x})$, which implicitly biases search toward near-stationary regions where improvement via stationarity is plausible (pathway (ii)).

4.5. Expected Improvement via Gradient Norms

Although the lower bound (6) reduces the intractability of EI_g to evaluating the gradient term EI_s in (7), EI_s remains impractical to compute within acquisition optimization. We therefore introduce a tractable approximation $\overline{\text{EI}}_s$ and use it to define the practical acquisition EI-GN .

To this end, we first define \mathbf{L} as the Cholesky decomposition for a positive definite covariance $\Sigma^\nabla(\mathbf{x}) \succ 0$ such

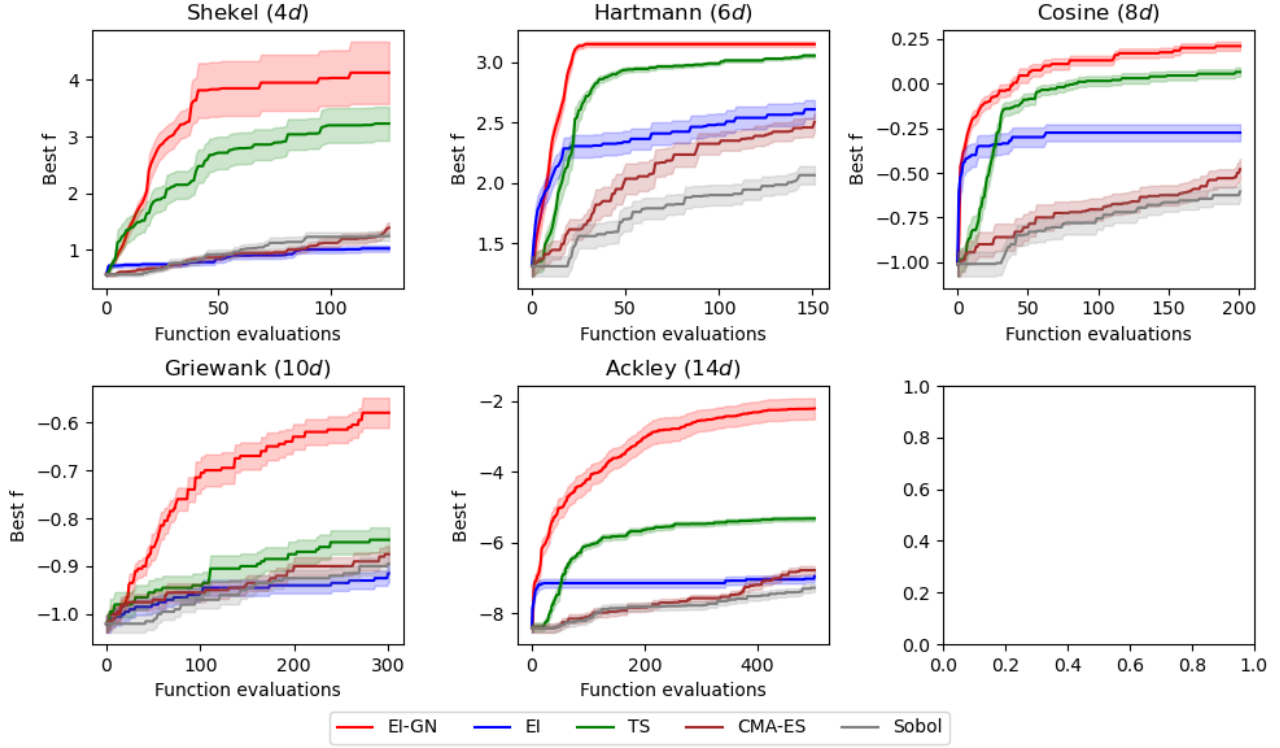


Figure 3. Results displaying mean \pm one standard error for synthetic benchmarks: Shekel (4d), Hartmann (6d), Cosine (8d), Griewank (10d), and Ackley (14d) for EI-GN against a variety of baselines.

that $\Sigma^\nabla(\mathbf{x}) = \mathbf{L}\mathbf{L}^\top$. Hence, we rewrite $\nabla f(\mathbf{x})$ via the whitening transformation: $\nabla f(\mathbf{x}) = \mu^\nabla(\mathbf{x}) + \mathbf{L}\mathbf{z}$, where $\mathbf{z} \sim \mathcal{N}(\mathbf{0}, \mathbf{I})$. This also permits a change of variables $\mathbf{z}^+ = \mathbf{L}^{-1}(\nabla f(\mathbf{x}^+) - \mu^\nabla(\mathbf{x}))$. Recall the independent modeling assumption from Section 4.1, which yields diagonal $\Sigma^\nabla(\mathbf{x})$ and \mathbf{L} , with distinct elements. This leads to the anisotropic case where $\|\nabla f(\mathbf{x})\|_2^2$ becomes a generalized noncentral chi-square variable

$$\text{EI}_s(\mathbf{x}) = \int_{\|\nabla f(\mathbf{x}^+)\|_2^2}^{\infty} (u - \|\nabla f(\mathbf{x}^+)\|_2^2) p_{g\chi'^2}(u) du, \quad (10)$$

where u denotes the random variable $\|\nabla f(\mathbf{x})\|_2^2$. Computing (10) is nontrivial since it does not have a closed-form. Methods such as characteristic function inversion (Imhof, 1961; Davies, 1980) use iterative numerical integration and are impractical to invoke repeatedly within AF optimization.

We recognize the difficulty of evaluating (10) stems from the non-separable truncation of $u = \|\mu^\nabla(\mathbf{x}) + \mathbf{L}\mathbf{z}\|_2^2$. Therefore, we adopt a mean-field approximation by substituting the coupled norm-based truncation with an orthant truncation anchored at the incumbent $\{\|\mu^\nabla(\mathbf{x}) + \mathbf{L}\mathbf{z}\|_2^2 \geq \|\nabla f(\mathbf{x}^+)\|_2^2\} \approx \{\mathbf{z} \geq_{\text{cw}} \mathbf{z}^+\}$, where \geq_{cw} denotes element-wise inequality. The orthant event is neither a subset nor a superset of the norm event, so it should be interpreted as a tractable approximation rather than a bound. We now define

$\overline{\text{EI}}_s$ as the mean-field approximation of EI_s

$$\overline{\text{EI}}_s(\mathbf{x}) = \int_{\mathbf{z}^+}^{\infty} (\|\mu^\nabla(\mathbf{x}) + \mathbf{L}\mathbf{z}\|_2^2 - \|\nabla f(\mathbf{x}^+)\|_2^2) \phi_{\mathbf{z}}(\mathbf{z}) d\mathbf{z}, \quad (11)$$

where $\phi_{\mathbf{z}}$ denotes the multi-variate PDF of \mathbf{z} . This yields separable truncated moments and a closed-form expression; see Appendix C.1 for the full derivation. We now define the acquisition EI-GN as

$$\text{EI-GN}(\mathbf{x}) = \text{EI}_f(\mathbf{x}) - \alpha \overline{\text{EI}}_s(\mathbf{x}). \quad (12)$$

The computational complexity of (12) is discussed in Appendix C.2, and its pseudocode is given in Algorithm 1.

Beyond tractability, the mean-field approximation preserves the intended stationarity bias by penalizing large gradients, but this is achieved on a per-dimension basis. In other words, we alter the order of operations: the positive-part truncation is first applied on per-dimension contributions then aggregated. This contrasts the norm-based generalized χ^2 approach, which aggregates across dimensions before applying truncation on the scalar u . The reordering induces a more *balanced* stationarity signal; the quadratic norm aggregation may allow one coordinate's contribution to u dominate, whereas the per-dimension approach places more emphasis on distributing the stationarity penalty across all coordinates.

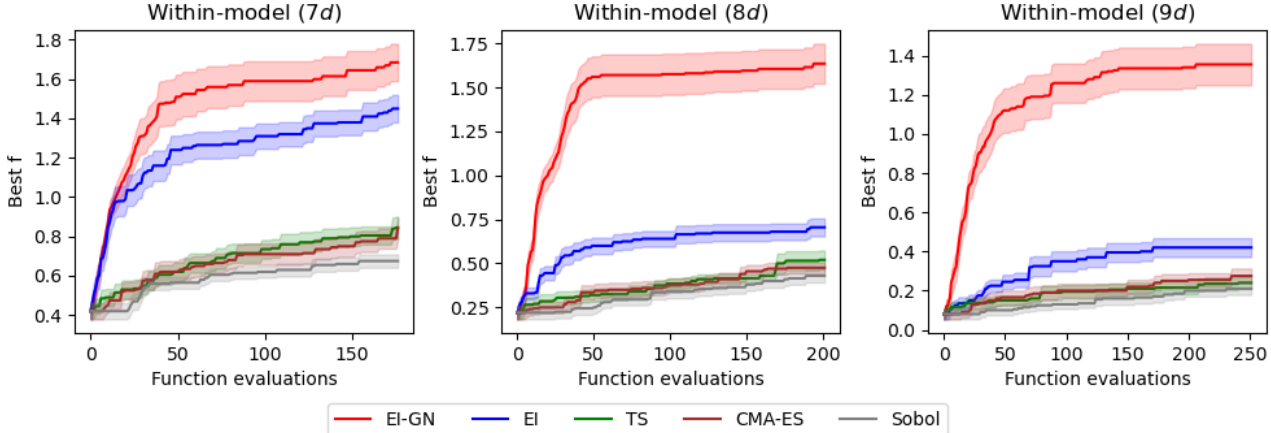


Figure 4. Results displaying mean \pm one standard error for within-model comparisons in 7d, 8d, and 9d.

5. Experiments

5.1. Experimental Setup

Each experiment is repeated across 20 seeds, initialized with 3d quasi-random Sobol points. All results are shown with mean \pm one standard error of best f . Unless stated otherwise, we model GPs with the Matérn-5/2 kernel along with Automatic Relevance Determination (ARD); additional implementation details can be found in Appendix D. We find that EI-GN performance is largely insensitive to α and use $\alpha = 0.6$ for all EI-GN experiments; hyperparameter tuning experiments for α can be found in Appendix E.1.

We consider two benchmark categories: synthetic benchmarks and GP samples. Here, the function and gradient observations are assumed to be deterministic to isolate acquisition behavior without confounding due to objective noise. We compare EI-GN against EI, Thompson Sampling (TS) (Daniel et al., 2018), CMA-ES (Hansen & Ostermeier, 2001), and Sobol. We use EI as the primary EI-family baseline since it is canonical and directly connected to our formulation (e.g., the $\alpha = 0$ special case) and defer comparisons to LogEI (Ament et al., 2023), a variant designed to mitigate EI's vanishing acquisition signal, to Appendix E.2. We also explore extinctions of EI-GN to policy search, where noisy objective and gradient observations are assumed.

5.2. Synthetic Benchmarks

We analyze performance across synthetic benchmarks that are generally difficult to optimize due to multimodality, across a range of dimensions: Shekel (4d), Hartmann (6d), Cosine (8d), Griewank (10d), Ackley (14d). These problems are standard in optimization literature and are commonly used to establish performance (Surjanovic & Bingham, 2014).

Figure 3 displays the results of EI-GN against the other baselines for the synthetic benchmarks. We observe EI-GN achieving strong performance with TS trailing behind for Shekel (4d), though the uncertainty in the former is relatively high, suggesting global maxima for this problem is difficult to locate due to objective landscape. This is supported by the relatively poor performance of the other baselines. For Hartmann (6d) and Cosine (8d), both EI-GN and EI have near identical performance in the first few BO iterations, but the latter stagnates soon after due to over-exploitation in local maxima. TS has worse performance than both initially, but eventually outperforms EI since it is more exploratory. As expected, it shows comparable performance to EI-GN overall since TS tends to perform well in these dimensions (Kandasamy et al., 2018). In Griewank (10d) and Ackley (14d), EI-GN has significant outperformance compared to the other baselines, highlighting the importance of gradient information when acquisition landscape becomes challenging to navigate. EI appears to have similar initial performance in Ackley (14d), but soon collapses to a local maxima.

The relative performance of each method is heavily affected by multimodality and flat regions of the objective function, and is not merely a function of dimensionality. As shown in synthetic benchmarks of moderate dimension (i.e., Hartmann (6d), Cosine (8d)), exploration-based AFs such as TS are competitive to avoid over-exploitation. However, they are insufficient for more complex objective landscapes (i.e. Griewank (10d), Ackley (14d)) where gradient information is necessary to effectively guide optimization in search space. Furthermore, the independent gradient-enhanced GPs ignore correlations and only yield approximate gradient inference, meaning the stationarity penalties are not operating under fully accurate gradient information.

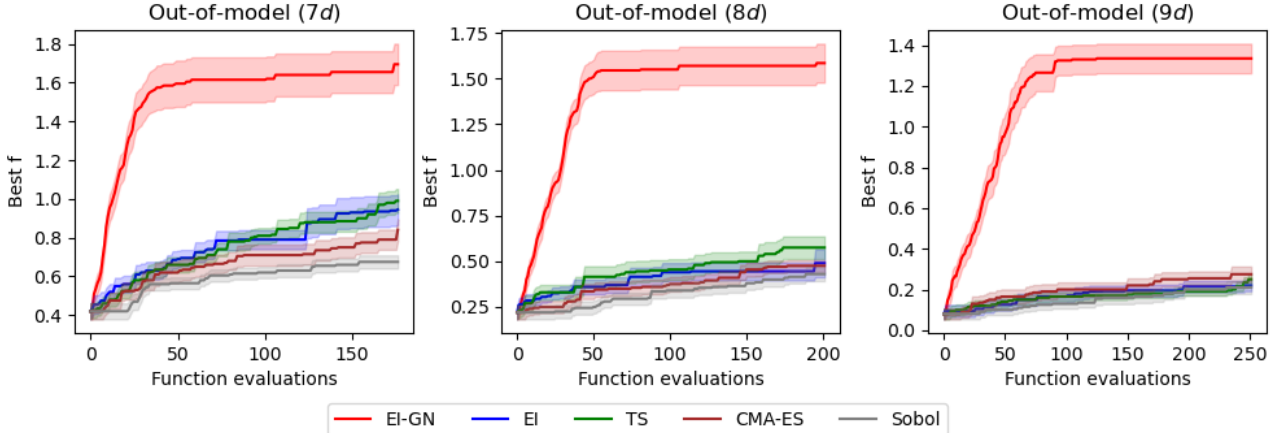


Figure 5. Results displaying mean \pm one standard error for out-of-model comparisons in 7d, 8d, and 9d.

5.3. GP samples

In GP samples, we consider both within-model comparisons (Hennig & Schuler, 2012) and out-of-model comparisons (Müller et al., 2021) in 7d, 8d, and 9d.

5.3.1. WITHIN-MODEL COMPARISONS

We analyze performance under within-model comparisons (Hennig & Schuler, 2012) to establish acquisition performance under idealized assumptions where model structure and hyperparameter mismatches are eliminated. This is achieved with objectives sampled via GP priors and can be considered the best-case regime for AFs of interest. This isolates the impact of gradient information in EI-GN to ascertain whether the stationarity penalty effectively guides optimization even when models are specified perfectly. In addition, the GP for f is blind to the gradient observations due to the structure of the gradient-enhanced GPs, therefore any performance gains must be solely due to the gradient-based term. We sample objectives from GP priors with RBF kernels and use the same kernel class in the surrogates to preserve matched model specification.

Figure 4 shows EI-GN outperforming all other baselines, suggesting acquisition behavior can be directly improved with gradient information to inform stationarity penalties rather than indirectly via improved surrogates. EI achieves similar results to EI-GN for 7d, but its performance degrades with 8d and 9d. This reinforces the prior claim that EI over-exploits, as even under perfect surrogate assumptions, sufficiently complex problem landscapes will eventually cause premature convergence to local maxima. TS underperforms both EI-GN and EI in the within-model comparisons, even though they had strong performance in the synthetic benchmarks for similar dimensions, indicating that dimensionality is not the sole factor for AF performance. Synthetic benchmarks tend to have many high-valued local

maxima, which favor exploration via posterior sampling. However, objectives sampled from GP priors may be multimodal, yet only contain relatively few high-reward basins; hence, TS suffers from these objective landscapes. In these regimes, structured exploration via stationarity penalties is more impactful than exploration via posterior sampling.

5.3.2. OUT-OF-MODEL COMPARISONS

Unlike within-model comparisons, the hyperparameters of the GP prior used to generate the objective and those in the surrogate for BO vary for out-of-model comparisons (Müller et al., 2021). This allows investigation of acquisition performance under model mismatch and hyperparameter optimization. However, this differs from traditional synthetic benchmarks since they maintain smooth GP-like objective landscapes while deviating from ideal model assumptions. Therefore, out-of-model comparisons provide a controlled, yet more realistic environment for benchmarking EI-GN, where the effect of stationarity penalties is investigated under smooth objectives (and gradients) with imperfect surrogates. We hold all experimental conditions from the within-model comparisons constant, except we revert back to the Matérn-5/2 kernel with ARD to introduce kernel mismatch.

In Figure 5, not only do we observe strong EI-GN results, its performance compared to the within-model comparisons is largely unchanged, highlighting the importance of gradient information. Furthermore, this also demonstrates that they are robust to approximate posteriors derived from uncorrelated surrogates and model misspecifications. On the other hand, EI underperforms and is on par with TS. When only informed on zeroth-order information, inaccurate beliefs of problem landscape can cause convergence to even more suboptimal basins. Although TS underperforms as well, its performance largely remains constant from the within

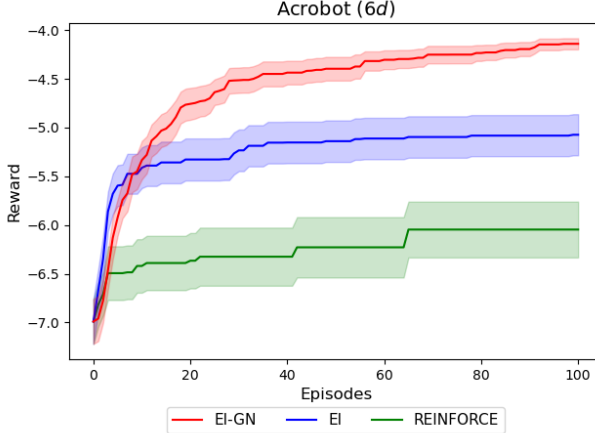


Figure 6. Mean \pm one standard error for Acrobot (6d) displayed for EI-GN (red), EI (blue), and REINFORCE (green).

model case. This can be attributed to it being less sensitive to model mismatches due to posterior sampling exploration; yet it retains similar performance to the within-model comparisons due to the same failure modes.

In both within and out-of-model comparisons, EI-GN consistently outperforms all other baselines, which can be attributed to the smooth, GP-like objectives leading to higher quality gradient observations. The stationarity penalty in EI-GN effectively drives optimization towards relevant regions of the search space, thereby speeding up discovery of desired maxima, even when uncorrelated models are approximate and offer no improvements to surrogate accuracy in f , as well as model mispecifications. Other acquisition functions must rely on zeroth order information only and cannot take advantage of gradient structure, triggering performance degradations with landscape complexity and model mismatches.

5.4. EI-GN Application to Policy Search

We now demonstrate EI-GN on solving policy search problems. Policy search methods aim to learn optimal parameters of a stochastic policy using noisy observations of a reward function. Since gradients of the expected reward are not directly observable, they are estimated using policy gradient theorem (Sutton et al., 1999).

Policy search is often performed using local stochastic gradient methods that rely on gradient directions and lack mechanisms for global exploration. BO has been used in policy search with strong sample efficiency, yet it treats the expected reward as a black-box objective. In contrast, trajectory-level signals can be exploited to improve policy search (Wilson et al., 2014). We position EI-GN as a hybrid approach that combines BO’s global exploration with gradient-based policy learning by directly incorporating

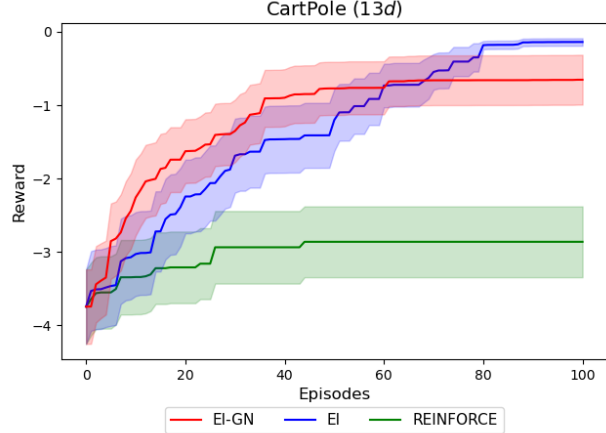


Figure 7. Mean \pm one standard error for Cartpole (13d) displayed for EI-GN (red), EI (blue), and REINFORCE (green).

policy gradient estimates—computed from the same rollouts used to estimate rewards—when proposing new policies. We compare EI-GN to EI and REINFORCE (Williams, 1992) as representative zeroth- and first-order methods, respectively, and evaluate performance on a linear policy in Acrobot (6d) (Sutton, 1995) and a neural policy in Cartpole (13d) (Barto et al., 1988).

As seen in Figure 6, EI-GN and EI have similar performance on Acrobot in early iterations, but EI then plateaus, suggesting sensitivity to local basins. EI-GN exhibits lower variance across seeds and reliably reaches higher rewards. For Cartpole shown in Figure 7, EI-GN and EI achieve similar performance, which is attributed to the reduced informativeness of policy gradients due to increased policy complexity and consequently higher-variance gradient estimation. In both problems, EI-GN is more sample-efficient than REINFORCE, but this comparison is intended only as a contrast to purely local first-order updates. We recognize that policy search methods are sensitive to design choices (i.e., learning rates, entropy regularization, gradient clipping).

6. Conclusion

We build upon EI by applying the improvement criterion to a gradient-aware auxiliary variable, mitigating its tendency toward over-exploitation. We derive a new acquisition function and present a closed-form approximation, EI-GN, for its computation. Through empirical evaluation on synthetic benchmarks, GP sample-based objectives, and policy search problems, we demonstrate that EI-GN achieves competitive performance. Future work will extend EI-GN to improve robustness under noisy objectives and gradient estimates.

Impact Statement

This paper presents work whose goal is to advance the field of Machine Learning. There are many potential societal consequences of our work, none which we feel must be specifically highlighted here.

References

Ament, S., Daulton, S., Eriksson, D., Balandat, M., and Bakshy, E. Unexpected improvements to expected improvement for bayesian optimization. *Advances in Neural Information Processing Systems*, 36:20577–20612, 2023.

Balandat, M., Karrer, B., Jiang, D., Daulton, S., Letham, B., Wilson, A. G., and Bakshy, E. Botorch: A framework for efficient monte-carlo bayesian optimization. *Advances in neural information processing systems*, 33:21524–21538, 2020.

Barto, A. G., Sutton, R. S., and Anderson, C. W. Neuronlike adaptive elements that can solve difficult learning control problems. In Anderson, J. A. and Rosenfeld, E. (eds.), *Neurocomputing: Foundations of Research*, pp. 535–549. MIT Press, Cambridge, MA, 1988.

Benjamins, C., Raponi, E., Jankovic, A., Doerr, C., and Lindauer, M. Self-adjusting weighted expected improvement for bayesian optimization. *arXiv preprint arXiv:2306.04262*, 2023.

Boyd, S. and Vandenberghe, L. *Convex optimization*. Cambridge university press, 2004.

Calandra, R., Seyfarth, A., Peters, J., and Deisenroth, M. P. Bayesian optimization for learning gaits under uncertainty: An experimental comparison on a dynamic bipedal walker. *Annals of Mathematics and Artificial Intelligence*, 76(1):5–23, 2016.

Daniel, J. R., Benjamin, V. R., Abbas, K., Ian, O., and Zheng, W. A tutorial on thompson sampling. *Foundations and trends in machine learning*, 11(1):1–99, 2018.

Davies, R. B. Algorithm as 155: The distribution of a linear combination of χ^2 random variables. *Applied Statistics*, pp. 323–333, 1980.

De Ath, G., Everson, R. M., Rahat, A. A., and Fieldsend, J. E. Greed is good: Exploration and exploitation trade-offs in bayesian optimisation. *ACM Transactions on Evolutionary Learning and Optimization*, 1(1):1–22, 2021.

Frazier, P. I. A tutorial on bayesian optimization. *arXiv preprint arXiv:1807.02811*, 2018.

Gardner, J., Pleiss, G., Weinberger, K. Q., Bindel, D., and Wilson, A. G. Gpytorch: Blackbox matrix-matrix gaussian process inference with gpu acceleration. *Advances in neural information processing systems*, 31, 2018.

Hansen, N. and Ostermeier, A. Completely derandomized self-adaptation in evolution strategies. *Evolutionary computation*, 9(2):159–195, 2001.

Hennig, P. and Schuler, C. J. Entropy search for information-efficient global optimization. *The Journal of Machine Learning Research*, 13(1):1809–1837, 2012.

Hernández-Lobato, D., Hernandez-Lobato, J., Shah, A., and Adams, R. Predictive entropy search for multi-objective bayesian optimization. In *International conference on machine learning*, pp. 1492–1501. PMLR, 2016.

Hoffman, M., Brochu, E., De Freitas, N., et al. Portfolio allocation for bayesian optimization. In *UAI*, volume 11, pp. 327–336, 2011.

Imhof, J.-P. Computing the distribution of quadratic forms in normal variables. *Biometrika*, 48(3/4):419–426, 1961.

Ip, J. H. S., Chakrabarty, A., Masui, H., Mesbah, A., and Romeres, D. Preference-based multi-objective bayesian optimization with gradients. In *NeurIPS 2024 Workshop on Bayesian Decision-making and Uncertainty*, 2024.

Ip, J. H. S., Chakrabarty, A., Mesbah, A., and Romeres, D. User preference meets pareto-optimality in multi-objective bayesian optimization. In *Proceedings of the AAAI Conference on Artificial Intelligence*, volume 39, pp. 20246–20254, 2025.

Jamil, M. and Yang, X.-S. A literature survey of benchmark functions for global optimisation problems. *International Journal of Mathematical Modelling and Numerical Optimisation*, 4(2):150–194, 2013.

Jones, D. R., Schonlau, M., and Welch, W. J. Efficient global optimization of expensive black-box functions. *Journal of Global optimization*, 13(4):455–492, 1998.

Kandasamy, K., Krishnamurthy, A., Schneider, J., and Póczos, B. Parallelised bayesian optimisation via thompson sampling. In *International conference on artificial intelligence and statistics*, pp. 133–142. PMLR, 2018.

Lookman, T., Balachandran, P. V., Xue, D., and Yuan, R. Active learning in materials science with emphasis on adaptive sampling using uncertainties for targeted design. *npj Computational Materials*, 5(1):21, 2019.

Makrygiorgos, G., Paulson, J. A., and Mesbah, A. Gradient-enhanced bayesian optimization via acquisition ensembles with application to reinforcement learning. *IFAC-PapersOnLine*, 56(2):638–643, 2023a.

Makrygiorgos, G., Paulson, J. A., and Mesbah, A. No-regret bayesian optimization with gradients using local optimality-based constraints: Application to closed-loop policy search. In *2023 62nd IEEE Conference on Decision and Control (CDC)*, pp. 20–25. IEEE, 2023b.

Makrygiorgos, G., Ip, J. H. S., and Mesbah, A. Towards scalable bayesian optimization via gradient-informed bayesian neural networks. *arXiv preprint arXiv:2504.10076*, 2025.

Müller, S., von Rohr, A., and Trimpe, S. Local policy search with bayesian optimization. *Advances in Neural Information Processing Systems*, 34:20708–20720, 2021.

Nguyen, Q., Wu, K., Gardner, J., and Garnett, R. Local bayesian optimization via maximizing probability of descent. *Advances in neural information processing systems*, 35:13190–13202, 2022.

Padidar, M., Zhu, X., Huang, L., Gardner, J., and Bindel, D. Scaling gaussian processes with derivative information using variational inference. *Advances in Neural Information Processing Systems*, 34:6442–6453, 2021.

Penubothula, S., Kamanchi, C., and Bhatnagar, S. Novel first order bayesian optimization with an application to reinforcement learning. *Applied Intelligence*, 51(3):1565–1579, 2021.

Qin, C., Klabjan, D., and Russo, D. Improving the expected improvement algorithm. *Advances in Neural Information Processing Systems*, 30, 2017.

Shahriari, B., Swersky, K., Wang, Z., Adams, R. P., and De Freitas, N. Taking the human out of the loop: A review of bayesian optimization. *Proceedings of the IEEE*, 104(1):148–175, 2015.

Shekhar, S. and Javidi, T. Significance of gradient information in bayesian optimization. In *International Conference on Artificial Intelligence and Statistics*, pp. 2836–2844. PMLR, 2021.

Solak, E., Murray-Smith, R., Leithead, W., Leith, D., and Rasmussen, C. Derivative observations in gaussian process models of dynamic systems. *Advances in neural information processing systems*, 15, 2002.

Surjanovic, S. and Bingham, D. Virtual library of simulation experiments: Test functions and datasets. Website, 2014. URL <https://www.sfu.ca/~ssurjano/>.

Sutton, R. S. Generalization in reinforcement learning: Successful examples using sparse coarse coding. *Advances in neural information processing systems*, 8, 1995.

Sutton, R. S., McAllester, D., Singh, S., and Mansour, Y. Policy gradient methods for reinforcement learning with function approximation. *Advances in neural information processing systems*, 12, 1999.

Williams, C. K. and Rasmussen, C. E. *Gaussian processes for machine learning*, volume 2. MIT press Cambridge, MA, 2006.

Williams, R. J. Simple statistical gradient-following algorithms for connectionist reinforcement learning. *Machine learning*, 8(3):229–256, 1992.

Wilson, A., Fern, A., and Tadepalli, P. Using trajectory data to improve bayesian optimization for reinforcement learning. *The Journal of Machine Learning Research*, 15(1):253–282, 2014.

Wu, J. and Frazier, P. The parallel knowledge gradient method for batch bayesian optimization. *Advances in neural information processing systems*, 29, 2016.

Wu, J., Poloczek, M., Wilson, A. G., and Frazier, P. Bayesian optimization with gradients. *Advances in neural information processing systems*, 30, 2017.

Wu, J., Chen, X.-Y., Zhang, H., Xiong, L.-D., Lei, H., and Deng, S.-H. Hyperparameter optimization for machine learning models based on bayesian optimization. *Journal of Electronic Science and Technology*, 17(1):26–40, 2019.

A. Positive Part Inequality

Lemma A.1. For real-valued A and B ,

$$\max(A - B, 0) \geq \max(A, 0) - \max(B, 0). \quad (13)$$

Proof. We perform case analysis on the signs of A, B .

Case 1: $A \geq 0, B \geq 0, \max(A, 0) - \max(B, 0) = A - B$.

If $A - B \geq 0, \max(A - B, 0) = A - B$, hence inequality holds with equality.

If $A - B < 0, \max(A - B, 0) = 0 > A - B$, hence inequality holds.

Case 2: $A \geq 0, B < 0, \max(A, 0) - \max(B, 0) = A$.

$\max(A - B, 0) = A - B$. Since $B < 0, A - B > A$, hence inequality holds.

Case 3: $A < 0, B \geq 0, \max(A, 0) - \max(B, 0) = -B \leq 0$.

$\max(A - B, 0) = 0$, hence inequality holds.

Case 4: $A < 0, B < 0, \max(A, 0) - \max(B, 0) = 0$.

If $A < B$, then $A - B < 0$ and $\max(A - B, 0) = 0$, hence the inequality holds with equality.

If $A \geq B$, then $A - B \geq 0$ and $\max(A - B, 0) = A - B \geq 0$, hence the inequality holds.

□

B. EI_g Lower Bound

B.1. Derivation of EI_g Lower Bound

We proceed to derive the expected improvement (EI) acquisition function on $g(\mathbf{x})$.

$$\text{EI}_g(\mathbf{x}) = \mathbb{E} [\max(g(\mathbf{x}) - g(\mathbf{x}^+), 0)] \quad (14a)$$

$$\text{EI}_g(\mathbf{x}) = \mathbb{E} [\max (f(\mathbf{x}) - f(\mathbf{x}^+) - \alpha(\|\nabla f(\mathbf{x})\|_2^2 - \|\nabla f(\mathbf{x}^+)\|_2^2), 0)] \quad (14b)$$

$$\text{EI}_g(\mathbf{x}) \geq \mathbb{E} [\max (f(\mathbf{x}) - f(\mathbf{x}^+), 0)] - \alpha \mathbb{E} [\max (\|\nabla f(\mathbf{x})\|_2^2 - \|\nabla f(\mathbf{x}^+)\|_2^2, 0)] \quad (14c)$$

where a lower bound is applied when it is expressed as a sum of two max operators, based on Positive Part Inequality (Lemma A.1). The first expectation corresponds to EI_f

$$\text{EI}_g(\mathbf{x}) \geq \text{EI}_f(\mathbf{x}) - \alpha \mathbb{E} [\max (\|\nabla f(\mathbf{x})\|_2^2 - \|\nabla f(\mathbf{x}^+)\|_2^2, 0)] \quad (15)$$

C. EI-GN

C.1. Derivation of EI-GN

We define \mathbf{L} to be the Cholesky decomposition for a positive definite covariance $\Sigma^\nabla(\mathbf{x}) \succ 0$ such that $\Sigma^\nabla(\mathbf{x}) = \mathbf{L}\mathbf{L}^\top$. Hence, we rewrite $\nabla f(\mathbf{x})$ via the whitening transformation

$$\nabla f(\mathbf{x}) = \mu^\nabla(\mathbf{x}) + \mathbf{L}\mathbf{z} \quad (16)$$

where $\mathbf{z} \sim \mathcal{N}(\mathbf{0}, \mathbf{I}_d)$. Therefore,

$$\mathbb{E} [\max (\|\nabla f(\mathbf{x})\|_2^2 - \|\nabla f(\mathbf{x}^+)\|_2^2, 0)] = \mathbb{E} [\max (\|\mu^\nabla(\mathbf{x}) + \mathbf{L}\mathbf{z}\|_2^2 - \|\nabla f(\mathbf{x}^+)\|_2^2, 0)] \quad (17)$$

$\|\nabla f(\mathbf{x})\|_2^2$ follows the generalized chi-square distribution

$$= \int_{\|\nabla f(\mathbf{x}^+)\|_2^2}^{\infty} (u - \|\nabla f(\mathbf{x}^+)\|_2^2) p_{g\chi'^2}(u) du, \quad (18)$$

where u denotes the random variable $\|\nabla f(\mathbf{x})\|_2^2$. We note that evaluation of this integral is prohibitively expensive, hence we approximation the norm-based truncation with the orthant truncation anchored at the incumbent (Section 4.5)

$$\left\{ \|\mu^\nabla(\mathbf{x}) + \mathbf{L}\mathbf{z}\|_2^2 \geq \|\nabla f(\mathbf{x}^+)\|_2^2 \right\} \approx \left\{ \mathbf{z} \geq_{\text{cw}} \mathbf{z}^+ \right\} \quad (19)$$

With (16), $\mathbf{z}^+ = \mathbf{L}^{-1}(\nabla f(\mathbf{x}^+) - \mu^\nabla(\mathbf{x}))$ and this yields

$$= \int_{\mathbf{z}^+}^{\infty} (\|\mu^\nabla(\mathbf{x}) + \mathbf{L}\mathbf{z}\|_2^2 - \|\nabla f(\mathbf{x}^+)\|_2^2) \phi_{\mathbf{z}}(\mathbf{z}) d\mathbf{z} \quad (20)$$

This can be expanded into 3 terms

$$= \int_{\mathbf{z}^+}^{\infty} (\mu^\nabla(\mathbf{x})^\top \mu^\nabla(\mathbf{x}) - \|\nabla f(\mathbf{x}^+)\|_2^2) \phi_{\mathbf{z}}(\mathbf{z}) d\mathbf{z} \quad (21a)$$

$$+ 2 \int_{\mathbf{z}^+}^{\infty} \mu^\nabla(\mathbf{x})^\top \mathbf{L}\mathbf{z} \phi_{\mathbf{z}}(\mathbf{z}) d\mathbf{z} \quad (21b)$$

$$+ \int_{\mathbf{z}^+}^{\infty} \mathbf{z}^\top \Sigma^\nabla(\mathbf{x}) \mathbf{z} \phi_{\mathbf{z}}(\mathbf{z}) d\mathbf{z} \quad (21c)$$

Since \mathbf{z} follows a standard normal multi-variate, the PDF $\phi_{\mathbf{z}}(\mathbf{z})$ can be expressed as a product of individual single-variate PDFs ϕ

$$\phi_{\mathbf{z}}(\mathbf{z}) = \prod_{i=1}^d \phi(z_i) \quad (22)$$

Subsequently, Fubini's theorem can be applied in integration accordingly, where

$$\int \phi_{\mathbf{z}}(\mathbf{z}) d\mathbf{z} = \int \prod_{i=1}^d \phi(z_i) dz_i = \prod_{i=1}^d \int \phi(z_i) dz_i \quad (23)$$

The constants can be taken out of the integral for the evaluation of (21a)

$$= (\mu^\nabla(\mathbf{x})^\top \mu^\nabla(\mathbf{x}) - \|\nabla f(\mathbf{x}^+)\|_2^2) \int_{\mathbf{z}^+}^{\infty} \phi_{\mathbf{z}}(\mathbf{z}) d\mathbf{z} \quad (24a)$$

$$= (\mu^\nabla(\mathbf{x})^\top \mu^\nabla(\mathbf{x}) - \|\nabla f(\mathbf{x}^+)\|_2^2) \prod_{i=1}^d \int_{z_i^+}^{\infty} \phi(z_i) dz_i \quad (24b)$$

$$= (\mu^\nabla(\mathbf{x})^\top \mu^\nabla(\mathbf{x}) - \|\nabla f(\mathbf{x}^+)\|_2^2) \prod_{i=1}^d \Phi(-z_i^+) \quad (24c)$$

where Φ denotes the single-variate CDF of a Gaussian distribution. As for (21b), we begin by factoring the constants w.r.t integration

$$2\mu^\nabla(\mathbf{x})^\top \mathbf{L} \int_{\mathbf{z}^+}^{\infty} \mathbf{z} \phi_{\mathbf{z}}(\mathbf{z}) d\mathbf{z} \quad (25a)$$

We evaluate the integral component-wise. For any $j \in [d]$,

$$\left[\int_{\mathbf{z}^+}^{\infty} \mathbf{z} \phi_{\mathbf{z}}(\mathbf{z}) d\mathbf{z} \right]_j = \int_{\mathbf{z}^+}^{\infty} z_j \phi_{\mathbf{z}}(\mathbf{z}) d\mathbf{z}. \quad (26)$$

We extract $\phi(z_j)$ and evaluate the corresponding integral separately, but the other terms correspond to the integral of the PDF

$$= \int_{z_j^+}^{\infty} z_j \phi(z_j) dz_j \times \prod_{i \neq j} \int_{z_i^+}^{\infty} \phi(z_i) dz_i \quad (27a)$$

$$= \phi(z_j^+) \prod_{i \neq j} \Phi(-z_i^+) \quad (27b)$$

We now define $\phi(\mathbf{z}^+) = [\phi(z_1^+), \dots, \phi(z_d^+)]^\top$ and $\Phi(-\mathbf{z}^+) = [\Phi(-z_1^+), \dots, \Phi(-z_d^+)]^\top$ as the vectorized PDF and CDF for \mathbf{z} . Subsequently, the element-wise division of these two vectors can be defined as

$$\mathbf{w} = \phi(\mathbf{z}^+) \oslash \Phi(-\mathbf{z}^+) \quad (28)$$

Therefore (21b) can now be expressed as

$$2\mu^\nabla(\mathbf{x})^\top \mathbf{Lw} \prod_{i=1}^d \Phi(-z_i^+) \quad (29)$$

(21c) can be expressed as the summation across $i, j = 1, \dots, d$

$$\int_{\mathbf{z}^+}^{\infty} \mathbf{z}^\top \Sigma^\nabla(\mathbf{x}) \mathbf{z} \phi_{\mathbf{z}}(\mathbf{z}) d\mathbf{z} = \sum_{i,j=1}^d \Sigma^\nabla(\mathbf{x})_{ij} \underbrace{\int_{\mathbf{z}^+}^{\infty} z_i z_j \phi_{\mathbf{z}}(\mathbf{z}) d\mathbf{z}}_{I_{ij}} \quad (30)$$

The evaluation of the integral I_{ij} falls under two categories: $i = j$, $i \neq j$. For the first case where $i = j$,

$$\int_{\mathbf{z}^+}^{\infty} z_i^2 \phi_{\mathbf{z}}(\mathbf{z}) d\mathbf{z} = \prod_{i \neq k} \Phi(-z_k^+) \int_{z_i^+}^{\infty} z_i^2 \phi(z_i) dz_i \quad (31)$$

We proceed with integration by parts with

$$u = z_i, \quad dv = z_i \phi(z_i) dz_i \quad \Rightarrow \quad du = dz_i, \quad v = -\phi(z_i)$$

$$\int_{z_i^+}^{\infty} z_i^2 \phi(z_i) dz_i = \left[-z_i \phi(z_i) \right]_{z_i^+}^{\infty} + \int_{z_i^*}^{\infty} \phi(z_i) dz_i \quad (32a)$$

$$= z_i^+ \phi(z_i^+) + \Phi(-z_i^+) \quad (32b)$$

Therefore,

$$\int_{\mathbf{z}^+}^{\infty} z_i^2 \phi_{\mathbf{z}}(\mathbf{z}) d\mathbf{z} = (z_i^+ \phi(z_i^+) + \Phi(-z_i^+)) \prod_{i \neq k} \Phi(-z_k^+) \quad (33)$$

The second case is where $i \neq j$

$$\int_{\mathbf{z}^+}^{\infty} z_i z_j \phi_{\mathbf{z}}(\mathbf{z}) d\mathbf{z} = \int_{z_i^+}^{\infty} z_i \phi(z_i) dz_i \times \int_{z_j^+}^{\infty} z_j \phi(z_j) dz_j \times \prod_{k \neq i, j} \int_{z_k^+}^{\infty} \phi(z_k) dz_k \quad (34a)$$

$$= \phi(z_i^+) \phi(z_j^+) \prod_{k \neq i, j} \Phi(-z_k^+) \quad (34b)$$

To combine these terms together to yield a matrix, we first construct the non-diagonal terms, which we obtained from solving the integral in the case where $i \neq j$.

$$\phi(z_i^+) \phi(z_j^+) \prod_{k \neq i, j} \Phi(-z_k^+) = \frac{\phi(z_i^+) \phi(z_j^+)}{\Phi(-z_i^+) \Phi(-z_j^+)} \prod_k \Phi(-z_k^+) \quad (35)$$

Upon inspection, the outer product of \mathbf{w} will yield the correct non-diagonal elements of said matrix

$$\mathbf{w} \mathbf{w}^\top \prod_k \Phi(-z_k^+) \quad (36)$$

We note that this will result in diagonal terms where the ii^{th} element corresponds to

$$\frac{\phi(z_i^+)^2}{\Phi(-z_i^+)^2} \prod_k \Phi(-z_k^+) \quad (37)$$

This can be expressed as

$$\mathbf{w} \odot \mathbf{w} \prod_k \Phi(-z_k^+) \quad (38)$$

and will need to be corrected when building the matrix. Now, we proceed with the diagonal terms. We return to the case where $i = j$ and rewrite the results by expanding the terms

$$(z_i^+ \phi(z_i^+) + \Phi(-z_i^+)) \prod_{i \neq k} \Phi(-z_k^+) = z_i^+ \phi(z_i^+) \prod_{i \neq k} \Phi(-z_k^+) + \prod_k \Phi(-z_k^+) \quad (39a)$$

$$= \left(1 + \frac{z_i^+ \phi(z_i^+)}{\Phi(-z_i^+)}\right) \prod_k \Phi(-z_k^+) \quad (39b)$$

Therefore, the corrected diagonal can be expressed as

$$(\mathbf{1} + \mathbf{z}^+ \odot \mathbf{w} - \mathbf{w} \odot \mathbf{w}) \prod_k \Phi(-z_k^+) \quad (40)$$

Combining the diagonal and non-diagonal terms into a matrix will yield

$$(\mathbf{w} \mathbf{w}^\top + \text{diag}(\mathbf{1} + (\mathbf{z}^+ - \mathbf{w}) \odot \mathbf{w})) \prod_i \Phi(-z_i^+) \quad (41)$$

Recall that (21c) requires the evaluation of

$$\sum_{i,j=1}^d \Sigma^\nabla(\mathbf{x})_{ij} I_{ij} \quad (42)$$

The element-wise multiplication and summation is the definition of the Frobenius inner product, which can also be expressed as the trace of the matrix products. Hence, (21c) becomes

$$\text{tr} \left(\Sigma^\nabla(\mathbf{x}) (\mathbf{w} \mathbf{w}^\top + \text{diag}(\mathbf{1} + (\mathbf{z}^+ - \mathbf{w}) \odot \mathbf{w})) \right) \prod_{i=1}^d \Phi(-z_i^+) \quad (43)$$

(21) is equivalent to

$$= \left(\prod_{i=1}^d \Phi(-z_i^+) \right) \left(\mu^\nabla(\mathbf{x})^\top \mu^\nabla(\mathbf{x}) - \|\nabla f(\mathbf{x}^+)\|_2^2 + 2\mu^\nabla(\mathbf{x})^\top \mathbf{L} \mathbf{w} \right) \quad (44a)$$

$$+ \text{tr} \left(\Sigma^\nabla(\mathbf{x}) (\mathbf{w} \mathbf{w}^\top + \text{diag}(\mathbf{1} + (\mathbf{z}^+ - \mathbf{w}) \odot \mathbf{w})) \right) \quad (44b)$$

The resulting optimizer of the acquisition function can be obtained from substituting the terms from (15)

$$\mathbf{x}_{t+1} \leftarrow \arg \max_{\mathbf{x}} (\mu(\mathbf{x}) - f(\mathbf{x}^+)) \Phi \left(\frac{\mu(\mathbf{x}) - f(\mathbf{x}^+)}{\sigma(\mathbf{x})} \right) + \sigma(\mathbf{x}) \phi \left(\frac{\mu(\mathbf{x}) - f(\mathbf{x}^+)}{\sigma(\mathbf{x})} \right) \quad (45a)$$

$$- \alpha \left(\prod_{i=1}^d \Phi(-z_i^+) \right) \left(\mu^\nabla(\mathbf{x})^\top \mu^\nabla(\mathbf{x}) - \|\nabla f(\mathbf{x}^+)\|_2^2 + 2\mu^\nabla(\mathbf{x})^\top \mathbf{L} \mathbf{w} \right) \quad (45b)$$

$$+ \text{tr} \left(\Sigma^\nabla(\mathbf{x}) (\mathbf{w} \mathbf{w}^\top + \text{diag}(\mathbf{1} + (\mathbf{z}^+ - \mathbf{w}) \odot \mathbf{w})) \right) \quad (45c)$$

C.2. Computational Complexity of EI-GN

Recall that EI-GN is comprised of two terms EI_f and $\overline{\text{EI}}_s$. Since the former corresponds to canonical EI, the complexity of this AF is dominated by $\overline{\text{EI}}_s$. Inspection of its closed-form expression in (44) shows it has complexity $O(d^2)$ due to matrix–vector products (e.g., $\mu^\nabla(\mathbf{x})^\top \mathbf{L} \mathbf{w}$) and quadratic forms/traces involving $\Sigma^\nabla(\mathbf{x})$.

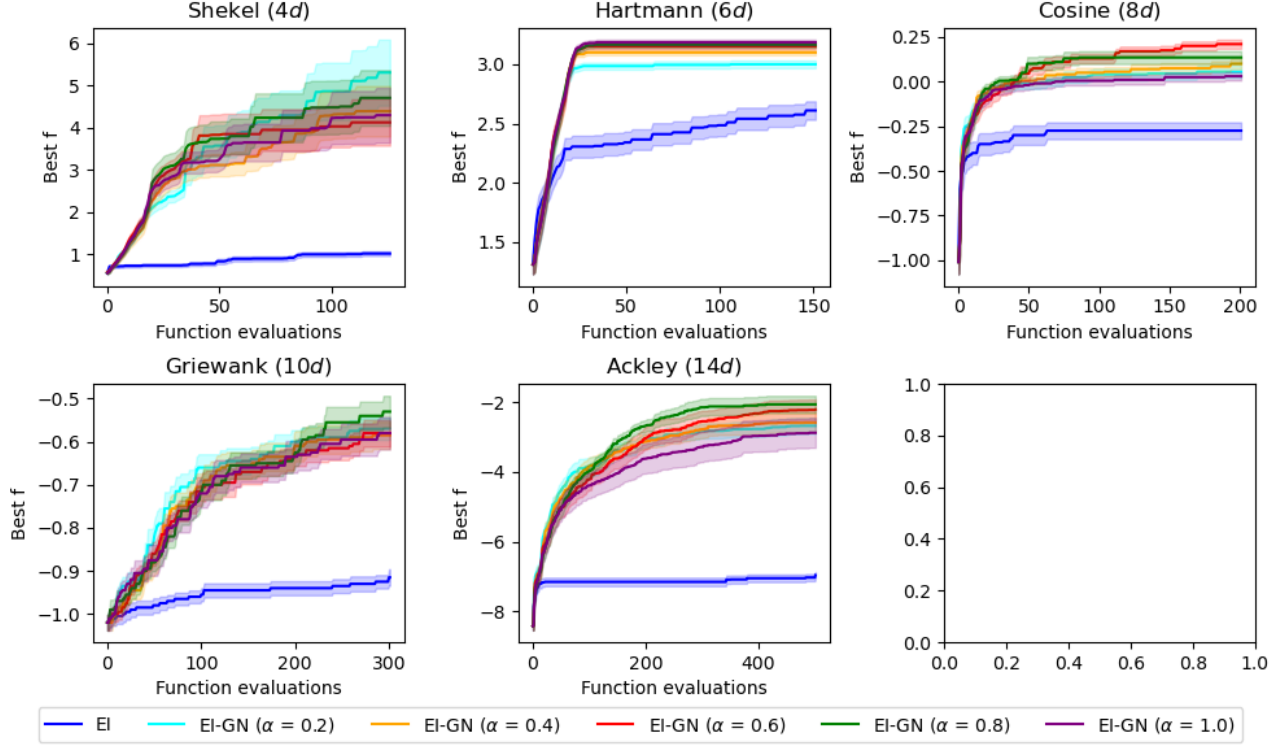


Figure 8. Hyperparameter tuning of $\alpha \in [0, 1]$ displayed with mean \pm one standard error for synthetic benchmarks: Shekel (4d), Hartmann (6d), Cosine (8d), Griewank (10d), and Ackley (14d). EI-GN with $\alpha = 0$ is displayed as EI for brevity.

However, since our implementation utilizes independent GPs that lead to diagonal posterior covariance $\Sigma^\nabla(\mathbf{x})$ (and hence diagonal \mathbf{L}). Under this diagonal structure, all terms decompose into elementwise sums (e.g., $\mu^\nabla(\mathbf{x})^\top \mathbf{L} \mathbf{w} = \sum_i \mu_i^\nabla(\mathbf{x}) (\mathbf{L})_{ii} w_i$ and $\text{tr}(\Sigma^\nabla(\mathbf{x}) \mathbf{w} \mathbf{w}^\top) = \sum_i (\sigma_i^\nabla(\mathbf{x}))^2 w_i^2$), so acquisition evaluation costs $O(d)$ per candidate \mathbf{x} , in addition to the cost of GP posterior evaluation.

In either case, the acquisition evaluation cost is typically negligible relative to GP posterior evaluation, which requires kernel evaluations and linear solves (e.g., Cholesky-based solves) whose cost is $\mathcal{O}(N^3)$. In the pessimistic scenario where the independent GPs cannot be trained or inferred in parallel, the cost can be up to $\mathcal{O}((d+1)N^3)$, which still results in negligible cost for EI-GN evaluation.

D. Implementation Details

D.1. Gaussian Processes

Our GP surrogates use the GPyTorch implementation (Gardner et al., 2018). Unless otherwise noted, we use a Matérn-5/2 kernel with ARD, with lengthscale hyperpriors $\text{LogNormal}(\log 0.4, 0.7)$ and outputscale hyperpriors $\text{Gamma}(2, 0.5)$. For within-model comparisons, we use an RBF kernel to match the GP prior used to sample the objective. Inputs are normalized to $[0, 1]^d$ and outputs are standardized to zero mean and unit variance.

To model gradient information, we fit d independent GP surrogates to the observed partial derivatives, one per coordinate of ∇y , using the same preprocessing and training procedure as for y . Each gradient GP has its own hyperparameters, fit by marginal likelihood, and provides posterior moments for $\nabla f(\mathbf{x})$ used in EI-GN. This choice treats f and ∇f as separate outputs and does not enforce the exact joint GP consistency constraints that arise from differentiating a single GP over f ; we adopt it for simplicity and scalability. In practice, gradient observations can span a large range of magnitudes, which can lead to occasional numerical issues in GP training. We therefore use an adaptive Cholesky jitter, increasing from 10^{-9} up to 10^{-2} only if factorization fails.

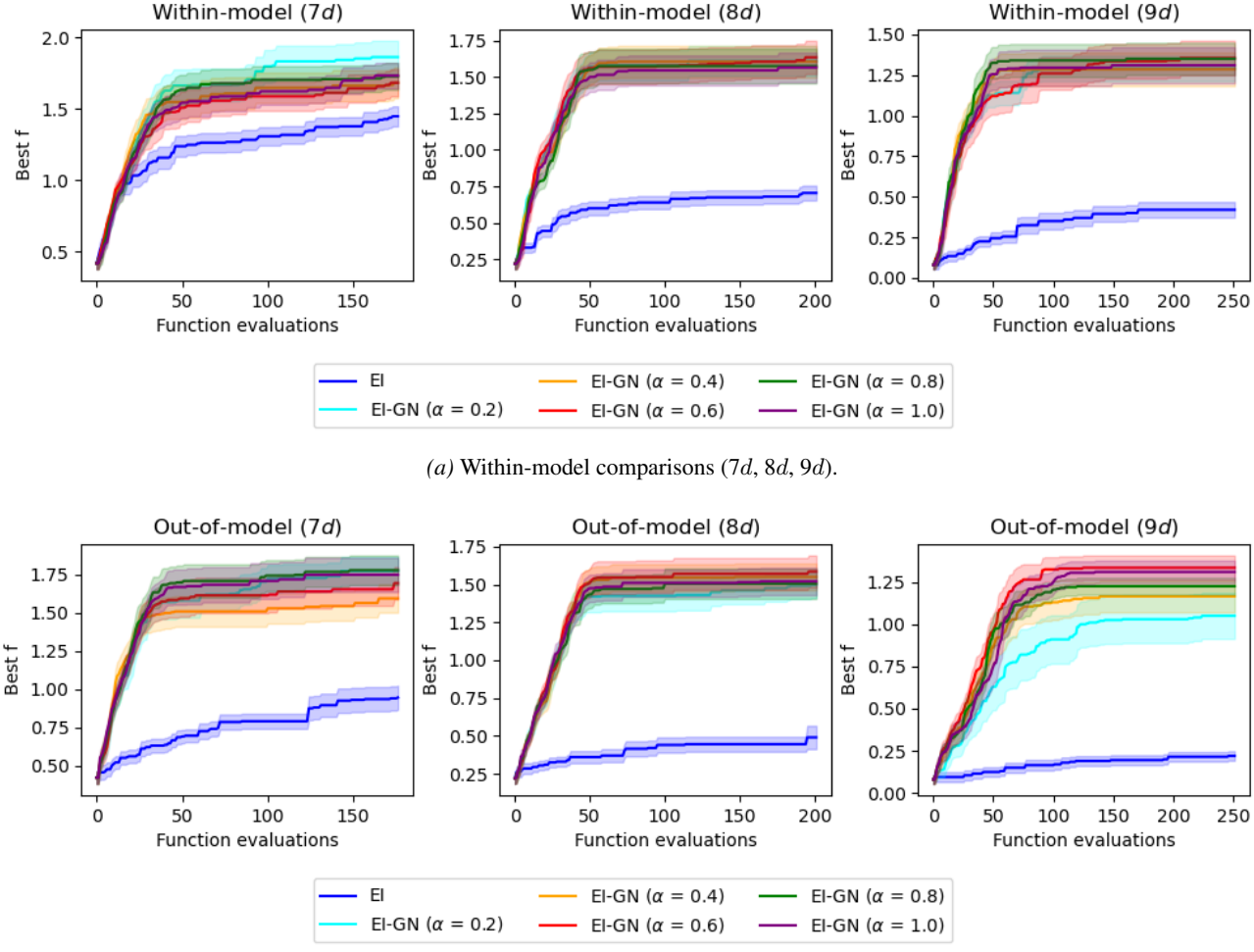


Figure 9. Hyperparameter tuning of $\alpha \in [0, 1]$ shown with mean \pm one standard error. EI-GN with $\alpha = 0$ is displayed as EI for brevity.

D.2. Acquisition Function Optimization

We implement EI-GN in BoTorch (Balandat et al., 2020) and maximize the acquisition using multi-start L-BFGS. We first generate a set of candidate points via Boltzmann sampling over the acquisition (raw samples), then select the top- k candidates as starting points (num restarts) for optimization.

D.3. Synthetic Benchmarks

We perform experiments across 20 seeds and report mean \pm one standard error for Shekel (4d), Hartmann (6d), Cosine (8d), Griewank (10d), and Ackley (14d) (Surjanovic & Bingham, 2014). Table 1 shows the implementation details for each of the synthetic benchmarks.

D.4. GP Samples

We use the objectives for within (Hennig & Schuler, 2012) and out of model comparisons (Müller et al., 2021), but create a separate one for each d . First, we create GP priors with RBF kernels, zero means, and lengthscales $0.4/\sqrt{d}$. $200d$ Sobol points in $[0, 1]^d$ are jointly sampled and GPs with the same hyperparameters are fit accordingly; the posterior means are treated as the black-box objective f . To maintain correct model specifications, we do not fit the surrogate between BO iterations for the within model comparisons, and also use the same hyperparameters as the GP prior. As for the out of model

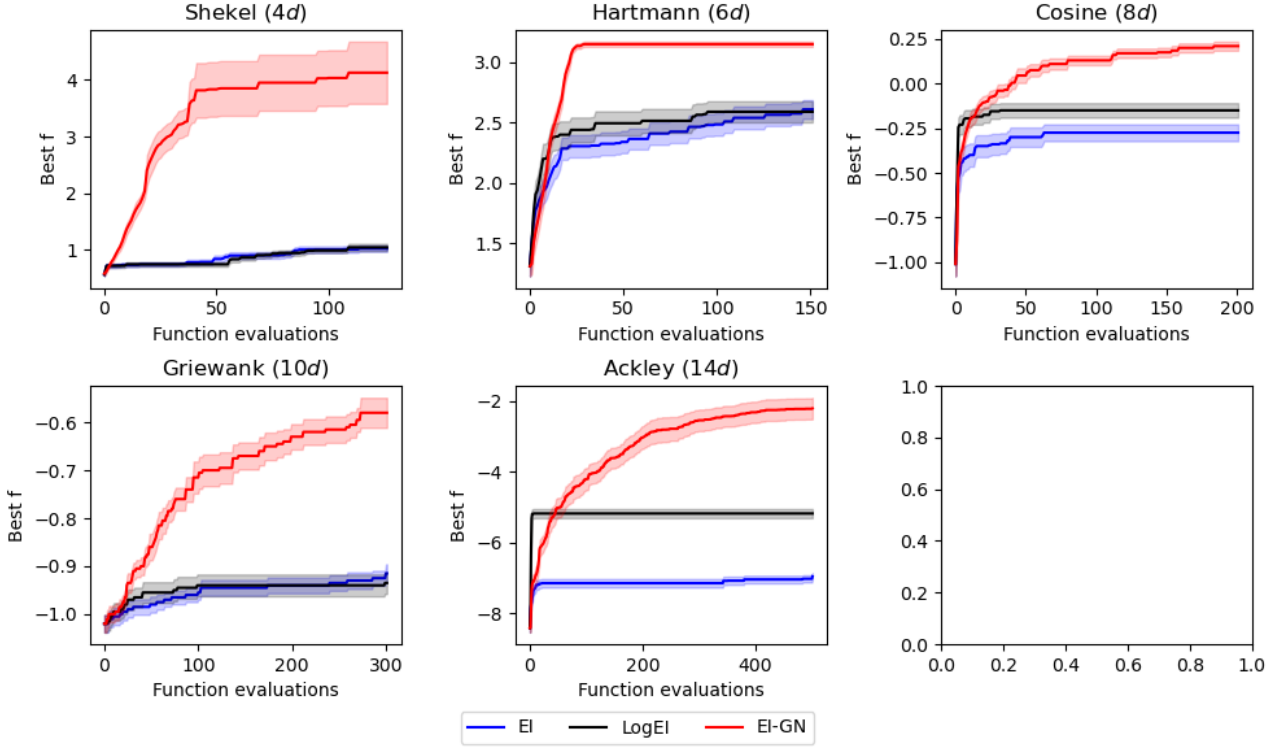


Figure 10. Comparison with LogEI displayed with mean \pm one standard error for synthetic benchmarks: Shekel (4d), Hartmann (6d), Cosine (8d), Griewank (10d), and Ackley (14d) for EI (blue), LogEI (black), and EI-GN (red). EI-GN corresponds to $\alpha = 0.6$.

comparisons, we revert to the Matérn-5/2 kernel with ARD, with lengthscale hyperpriors $\text{LogNormal}(\log 0.4, 0.7)$ and outputscale hyperpriors $\text{Gamma}(2, 0.5)$. Table 2 summarizes the within and out of model comparison implementation details.

D.5. Policy Search

We use stochastic policies and estimate gradients with the policy gradient theorem. To reduce estimated variance, we subtract a baseline given by the rollout-average return.

$$\nabla_{\theta} J \approx \frac{1}{M} \sum_{i=1}^M (R_i - \bar{R}) \nabla_{\theta} \log \pi_{\theta}(\tau_i),$$

where $\bar{R} = \frac{1}{N} \sum_i R_i$ is the mean return across M rollouts.

D.5.1. ACROBOT

Acrobot (Sutton, 1995) is a two-link pendulum swing-up task. We modify the reward to an via energy-based shaping

$$r = -0.001 (\cos(\theta_1) + \cos(\theta_1 + \theta_2)),$$

which provides a dense signal that correlates with the height of the end-effector and stabilizes policy-search optimization compared to sparse, goal-only rewards. This shaping preserves the swing-up objective (maximized when the links are upright) while yielding a smoother return landscape for global optimization methods.

The observation space is 6-dimensional: $[\cos \theta_1, \sin \theta_1, \cos \theta_2, \sin \theta_2, \dot{\theta}_1, \dot{\theta}_2]$, while we use a bounded linear policy: $a = \tanh(\mathbf{o}^T \mathbf{w})$, where $\mathbf{w} \in \mathbb{R}^6$, yielding a 6-dimensional search space. Episodes run for 500 steps with 32 Monte Carlo rollouts for gradient estimation. The policy noise standard deviation is $\sigma_{\pi} = 0.05$. Parameter bounds are $[-1, 1]^6$. We initialize with 18 Sobol points and set a budget of 100 episodes. For EI-GN and EI, we use 32 restarts and 512 raw samples for AF optimization.

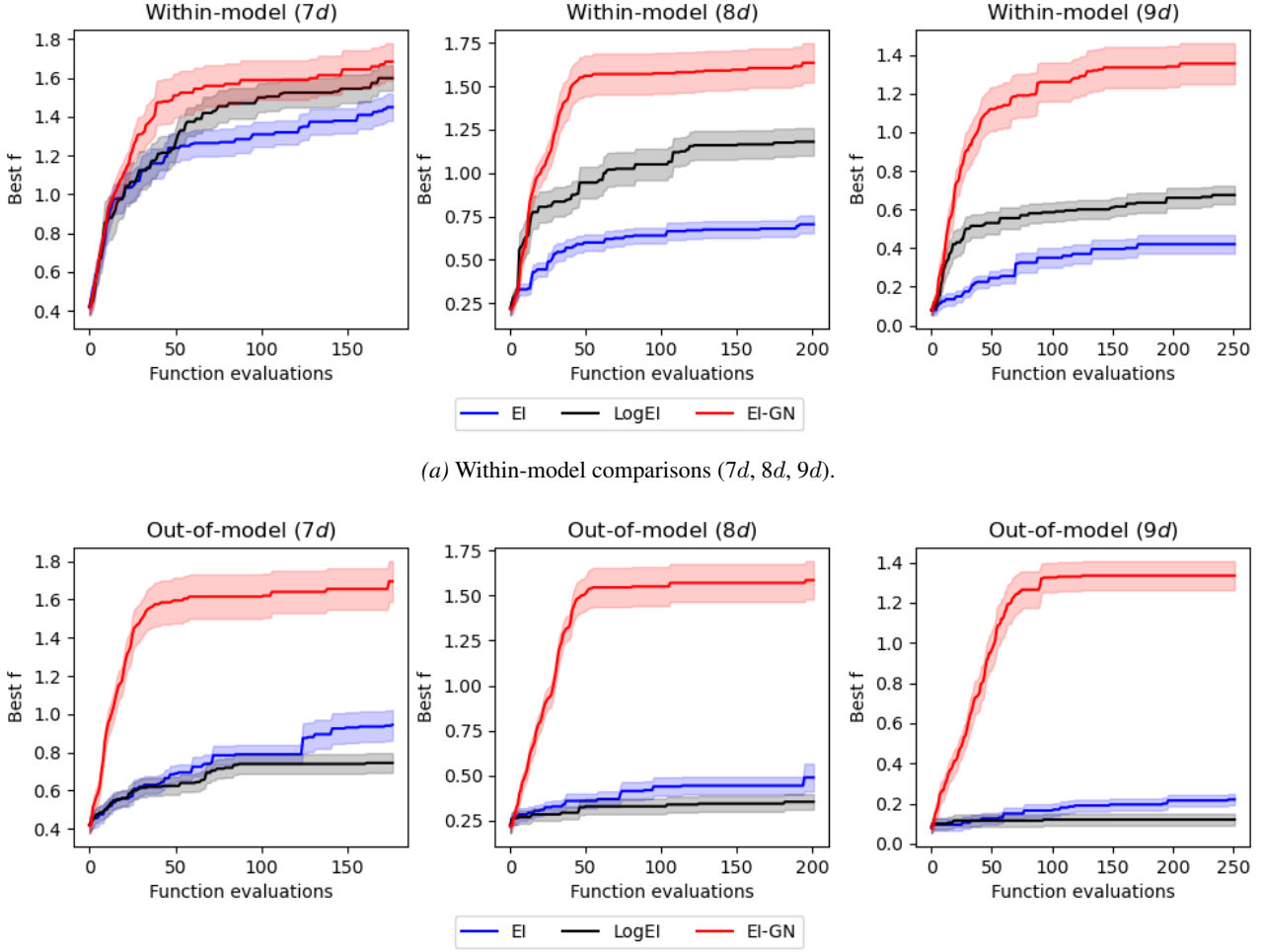


Figure 11. Comparison with LogEI (mean \pm one standard error). Curves show EI (blue), LogEI (black), and EI-GN (red); EI-GN uses $\alpha = 0.6$.

D.5.2. CARTPOLE

CartPole (Barto et al., 1988) is a control balancing task with a 4-dimensional observation: $[x, \dot{x}, \theta, \dot{\theta}]$ (cart position, cart velocity, pole angle, angular velocity). We replace the sparse survival reward with a quadratic shaping cost around the upright equilibrium,

$$r = - \left(\theta_t^2 + 0.1 \dot{\theta}_t^2 + 0.01 x_t^2 + 0.001 \dot{x}_t^2 + 0.001 a_t^2 \right),$$

which yields a smooth, dense return signal for continuous policy optimization. Termination conditions and dynamics follow the standard CartPole balancing setup; the modification affects only the reward signal used to define the policy-search objective. We use a 1-hidden-layer neural policy with 2 hidden units and ReLU activation:

$$a = \tanh(\text{ReLU}(\mathbf{o}^\top \mathbf{w}_1 + \mathbf{b}_1)^\top \mathbf{w}_2 + \mathbf{b}_2),$$

where $\mathbf{w}_1 \in \mathbb{R}^{4 \times 2}$, $\mathbf{b}_1 \in \mathbb{R}^2$, $\mathbf{w}_2 \in \mathbb{R}^2$, and $\mathbf{b}_2 \in \mathbb{R}$. This yields a 13-dimensional search space. Episodes run for 200 steps with 48 rollouts. Parameter bounds are $[-2, 2]^{13}$. 39 initial Sobol points are used and it is run for 100 episodes. AF optimization is done via 32 restarts and 512 raw samples.

E. Ablations

E.1. Hyperparameter tuning for α

In implementation, the objective-improvement and stationarity components can differ substantially in scale across problems and across BO iterations. During acquisition maximization, we apply an online rescaling of the objective-improvement and stationarity components using mean and standard deviation computed over the optimizer’s temporary candidate pool at each BO iteration to keep magnitudes comparable and improve numerical stability. The scaling does not eliminate the role of α , but makes a consistent sweep over $\alpha \in [0, 1]$ meaningful across tasks. We focus on this range since $\alpha = 0$ recovers EI and larger values place progressively greater emphasis on the stationarity component within the normalized acquisition; we did not find additional benefit outside this range in our tuning sweeps.

Figures 8, 9 show EI-GN with different α ; when $\alpha = 0$, the lack of gradient information leads to over-exploitation and subpar performance, as expected of EI. All other trajectories with positive α generally achieve similar performance, suggesting the weight of the hyperparameter is largely insignificant. However, EI-GN ($\alpha = 0.2$) for out of model (9d) comparisons in Figure 9b underperforms compared to $\alpha \geq 0.4$. Out of all the GP sample-based benchmarks, this problem has the most challenging objective landscape and optimization conditions, indicating a greater weight on the gradient-term is necessary.

E.2. Comparison with LogEI

We also seek to benchmark performance of EI-GN against LogEI, a modern EI variant designed to mitigate EI’s vanishing acquisition signal. In Figure 10, we observe generally similar performance between EI and LogEI except for Ackley (14d). However, both methods plateau after finding a local maxima, though LogEI consistently finds ones corresponding to larger values. Here, EI-GN still outperforms the other AFs.

In within model comparisons as seen in Figure 11a, LogEI has similar performance to EI for 7d, but outperforms the latter in 8d and 9d. Under idealized optimization assumptions, LogEI can derive greater acquisition signal and alleviate over-exploitation under sufficiently complex objectives. Although LogEI has marked improvement over EI, EI-GN still remains competitive. As for out-model-comparisons (Figure 11b), LogEI mostly collapses to EI in performance, indicating it is more likely to over-exploit when there is model mismatch. Similar to the case with synthetic benchmarks, EI-GN outperforms the other AFs.

Function	d	Initial points	Budget	Input space	Raw samples	Num restarts
Shekel	4	12	125	$[0, 10]^4$	8	256
Hartmann	6	18	150	$[0, 1]^6$	10	512
Cosine	8	24	200	$[-1, 1]^8$	20	1024
Griewank	10	30	300	$[-10, 10]^{10}$	20	1024
Ackley	14	42	500	$[-5, 5]^{14}$	20	1024

Table 1. Synthetic benchmark implementation details for Shekel (4d), Hartmann (6d), Cosine (8d), Griewank (10d), and Ackley (14d). For functions defined as minimization problems, we negate the objective for maximization.

Function	d	Initial points	Budget	Kernel	Raw samples	Num restarts
Within	7	21	175	RBF	10	512
Within	8	24	200	RBF	20	1024
Within	9	27	250	RBF	20	1024
Out	7	21	175	Matérn-5/2	10	512
Out	8	24	200	Matérn-5/2	20	1024
Out	9	27	250	Matérn-5/2	20	1024

Table 2. Implementation details for within and out of model comparisons in 7d, 8d, and 9d.